Scaling behaviors of the voltage distribution in dielectric breakdown networks

J. S. Lee and B. Kahng*

Department of Physics and Astronomy, Seoul National University, Seoul 151-747, Korea

(Received 10 January 2011; revised manuscript received 7 March 2011; published 5 May 2011)

We study the distribution of voltage drops across bonds in dielectric breakdown networks and its qth moments in the two-dimensional Euclidean space. Performing numerical simulations, we find that the distribution is composed of three different power-law regimes which are distinguished by two crossover voltages V_1 and V_2. The scaling behaviors of these crossover voltages with respect to the system size govern those of the qth moments of the voltage distribution. This feature differs from the multifractal behavior of the qth moment in random resistor networks. We discuss the implications of these scaling behaviors in relation to the application of the dielectric breakdown network to memory devices.

DOI: 10.1103/PhysRevE.83.052103 PACS number(s): 64.60.al, 64.60.ah, 05.45.Df

The percolation theory has played an important role in studying transport phenomena in heterogeneous media composed of conductors and insulators [1]. In ordinary percolation systems, a cluster is formed statically in the sense that randomly positioned conductors are connected when they locate at the nearest neighbors, creating connected (conducting) or disconnected (insulating) paths.

To understand transport properties in such a static percolation system, a random resistor network model [2–6] has been extensively studied, in which insulating and conducting bonds are located randomly. For this network rich structural and transport properties of the percolating cluster near percolation threshold have been uncovered. Of particular interest is the probability distribution $n(V)$ of voltage V in the percolating cluster of the random resistor network and the qth moment of voltage, $M_q \equiv \sum_V N(V)V^q$, where $N(V)$ is the number of bonds biased by a voltage V and $N(V) = M_0 n(V)$ by definition. Note that some of these moments provide physical information of the network [7–9]. The zeroth moment is the number of bonds carrying a current, that is, the mass of the backbone; the second and the fourth moment describe the resistance and the level of noise (or the third harmonic signal) of the whole network, respectively. One central interesting feature of the voltage distribution is its multiscaling or multifractal properties [3–6,10,11]; a conventional scaling approach or constant gap scaling law fails to describe the distribution, instead infinite set of exponents are needed to characterize it properly. In other words, the multifractality of the distribution can be probed by nonlinearly q-dependent exponent with respect to the system size L, that is, $M_q \sim L^{-p(q)/\nu}$, where $p(q)$ is a nonlinear function of q.

On the other hand, a percolating cluster can be formed dynamically by bond-switching mechanism between conducting and insulating bonds. One typical example is the dielectric breakdown network [12,13]. Opposite from the fuse network [14,15], in the dielectric breakdown network an insulating or a high resistive bond changes to a conducting or a low resistive bond when voltage across the insulating bond exceeds some threshold voltage $v_{\rm th}$. This "antifuse" switching occurs iteratively, which eventually results in a percolating dielectric breakdown network. Recently, this dielectric breakdown network has attained much attention [13,16–19] due to the potential application for the next nonvolatile high-density random access memory. It is manifest that transport properties of this type of memory depend on the voltage distribution, which can be different from those of the static percolation model created through random static processes. In spite of such potential implications, the voltage distribution of the dielectric breakdown network has not been studied yet. In this Brief Report, we study the properties of the voltage distribution of the dielectric breakdown network using numerical simulations.

We first explain how the dielectric breakdown network is generated. We consider a resistor network as shown in Fig. 1(a). Note that we used $L \times L$ square lattices for these numerical simulations. Each bond can have either one of two resistance values, r_h or r_l, where $r_h \gg r_l$. Let us assume that the r_h and r_l bonds are in off-state (insulating) and on-state (conducting), which are marked as thin (black) and thick (red) lines, respectively. An initial insulating configuration is mostly composed of off-state bonds, with a few on-state bonds with small fraction p_f as a defect. Here these defects give rise to random fluctuations of the voltage distribution, which is indispensable for generating a localized dielectric breakdown network. The top and bottom edges are connected to bus bars on which external voltage $V_{\rm ext}$ is applied. We calculated the voltage distribution using the standard over-relaxation method and used periodic boundary conditions in the transverse direction with $p_f = 0.1$, $v_{\rm th} = 0.1$, and $r_h/r_l = 10^5$. The system size L is various.

When external voltage is applied to the network and increased from zero, no resistance change happens until $V_{\rm ext}$ reaches a threshold voltage at which dielectric breakdown occurs as shown in Fig. 1(b). At this dielectric breakdown voltage, an insulating bond switches to the conducting bond depending on the voltage across the bond and it triggers an avalanche of switchings in other bonds nearby, which results in a percolating dielectric breakdown network. This avalanche process is presented in Figs. 1(c), 1(d), and 1(e), which are snapshots of the simulation after the fourth, seventh, and eighth iterations, respectively. As shown in Fig. 1(e), the percolating cluster is composed of singly connected bonds or links and multiply connected bonds or "blobs."

*bkahng@snu.ac.kr

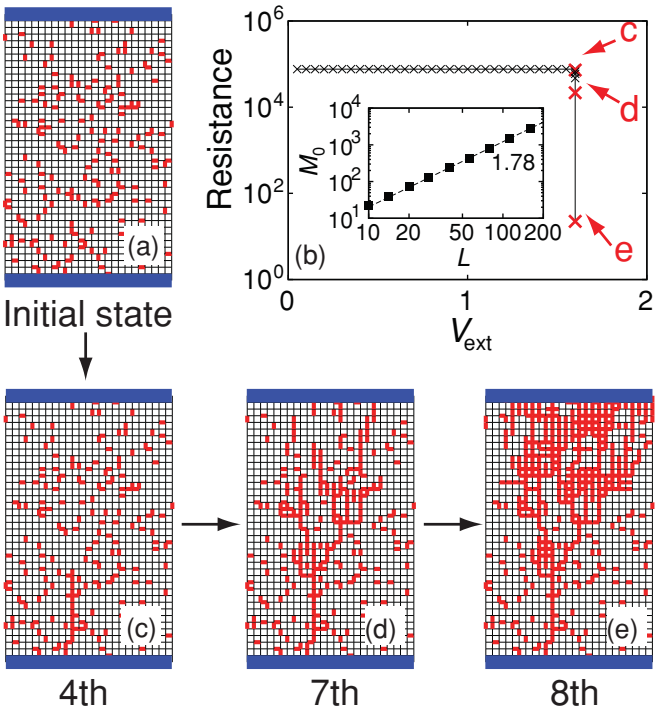

FIG. 1. (Color online) Generation of the dielectric breakdown network. (a) Initial insulating configuration where r_h (off-state) and r_l (on-state) bonds are marked as thin (black) and thick (red) lines, respectively. The top and bottom blue edges are bus bars on which external voltage V_{ext} is applied. (b) No resistance change happens until V_{ext} reaches a threshold voltage where dielectric breakdown occurs. Snapshots of the points c, d, and e are presented in (c), (d), and (e), respectively. (Inset) The size dependence of the zeroth moment M_0 of the voltage distribution.

Inset of Fig. 1(b) shows the size dependence of the number of the bonds carrying a current in a percolating network, that is, the zeroth moment M_0 of the voltage distribution when the electric current is permitted to flow only through on-state bonds. As shown in the figure, the number of bonds is proportional to size in a power-law manner, $M_0 \sim L^{D_f}$, which indicates the fractal properties of the percolating cluster of the dielectric breakdown network.

The voltage distribution $n(V)$ is built up by recording the absolute value of the voltage drops in all the bonds when a unit potential drop is imposed across the top and bottom edges of the percolating backbone network and then being normalized by the number of realizations of the network and also by the number of bonds in the backbone. Figure 2 shows the voltage distribution with $L = 160$ averaged over 600 realizations. The distribution can be divided into three regions which are distinguished by two crossover voltages V_1 and V_2. As the figure shows, the distributions of Regions 1 and 2 fit the power laws with different exponents $-\gamma_1$ and $-\gamma_2$, respectively. In Region 3, although it is difficult to conclude that it clearly represents a certain type of scaling function because of a short range of V, we assume that it also follows a power law with a large exponent $-\gamma_3$. Later we show that the choice of the scaling function for Region 3 has no influence on the scaling behavior of the qth moment. Then, considering the continuity of the distribution we can write the voltage distribution of size L as

$$n(V) \approx \begin{cases} C(L)V^{-\gamma_1} & \text{(Region1)}, \\ C(L)V_1^{\gamma_2-\gamma_1}V^{-\gamma_2} & \text{(Region2)}, \\ C(L)V_1^{\gamma_2-\gamma_1}V_2^{\gamma_3-\gamma_2}V^{-\gamma_3} & \text{(Region3)}, \end{cases} \quad (1)$$

where $C(L)$ is a size dependent coefficient. These multiple scaling behaviors of the voltage distribution are different from that of the random resistor network. For comparison, we present the logarithmic voltage distributions of both the random resistor network near percolation threshold and the dielectric breakdown network in the inset of Fig. 2. While multifractal behaviors of positive moments in the random resistor network mainly come from the high-voltage region in which the distribution drops abruptly, no such behavior appears in the voltage distribution of the dielectric breakdown network which can be seen further in detail by investigating the size dependence of the voltage distribution below. For this study, we have performed numerical simulations on the lattices with various sizes from $L = 10$ to $L = 160$. To obtain the voltage distribution, we average 10^4 realizations for sizes from $L = 10$ to $L = 80$, 2400 configurations for $L = 112$, and 600 realizations for $L = 160$. Figure 3(a) shows the size dependent voltage distribution. As the figure shows, three scaling regions become more distinctive as the size increases and $C(L)$ is a increasing function of L. Figures 3(b), 3(c), and 3(d) show the size dependence of the exponents γ_1, γ_2, and γ_3. From Figs. 3(b) and 3(c), it seems that the exponents γ_1 and γ_2 converge to 0.19 and 1.73 in the thermodynamic limit. For Region 3 it is hard to estimate the exponent γ_3 due to the large fluctuation coming from the too-large exponent magnitude; however, it seems that it also approaches roughly to 12. Figure 3(e) shows the dependence of the crossover voltages V_1 and V_2 on the system size. They have scaling relations as follows:

$$V_1 \sim L^{-\alpha} \quad \text{and} \quad V_2 \sim L^{-\beta}, \quad (2)$$

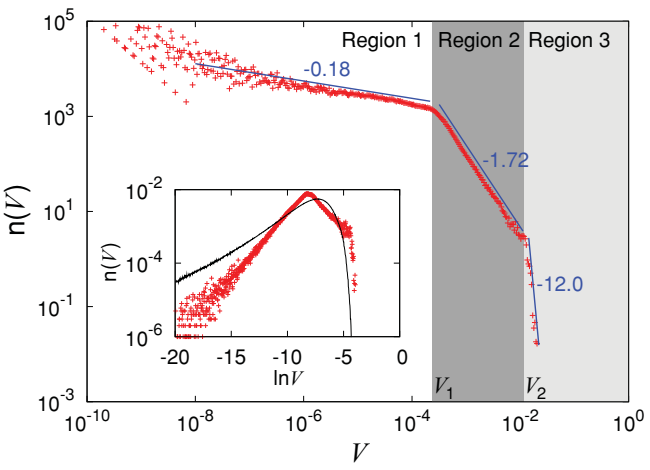

FIG. 2. (Color online) The voltage distribution of the dielectric breakdown network with the system size $L = 160$. Three regions are distinguished by two crossover voltages V_1 and V_2. Values of the slopes are denoted beside the guide lines. (Inset) The logarithmic voltage distributions of the random resistor network near percolation threshold (black line) and the dielectric breakdown network (red crosses).

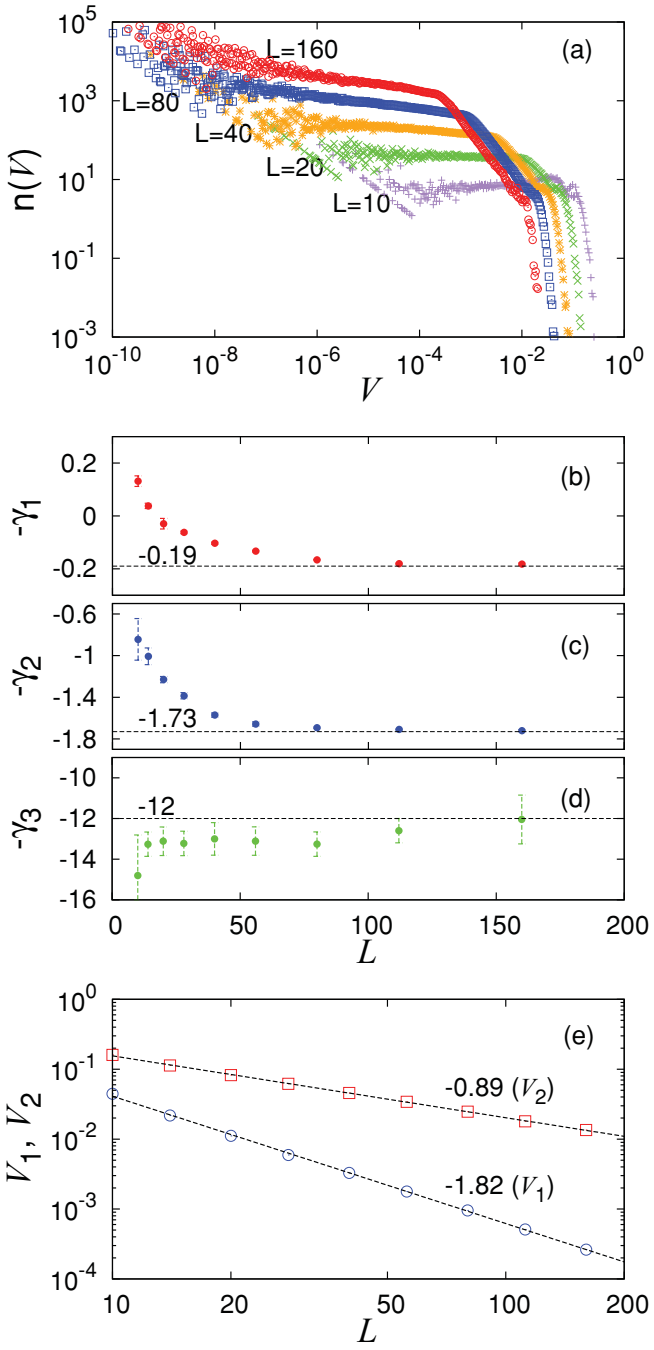

FIG. 3. (Color online) (a) Size dependence of the voltage distribution. Data for $L = 10$, 20, 40, 80, and 160 are denoted by $+$ (purple), $\times$ (green), $*$ (orange), $\square$ (blue), and $\circ$ (red), respectively. (b), (c), and (d) Size dependence of the exponents γ_1, γ_2, and γ_3. (e) Size dependence of the crossover voltages V_1 and V_2, which are denoted by $\circ$ (blue) and $\square$ (red), respectively. The slopes for V_1 and V_2 are -1.82 and -0.89, respectively.

where $\alpha \approx 1.82$ and $\beta \approx 0.89$.

Now let us consider how this multiple scaling property affects the behaviors of the qth moment of the voltage distribution; this can be achieved by the approximate transformation of the discrete summation $M_0 \sum_q n(V)V^q$ to the continuous integration $M_0 \int dV n(V)V^q = M_0(\int_{R1} + \int_{R2} + \int_{R3})dV n(V)V^q$, where R1, R2, and R3 denote the Regions 1, 2, and 3, respectively. The dominant term of this integration depends on the q value. Let us first consider the case $\gamma_1 - 1 < q < \gamma_2 - 1$ to determine the coefficient $C(L)$. Using Eqs. (1) and (2), we obtain

$$M_q/M_0 = C(L)L^{-\alpha(q-\gamma_1+1)}, \quad (\gamma_1 - 1 < q < \gamma_2 - 1).$$

Since $\gamma_1 \approx 0.19$ and $\gamma_2 \approx 1.73$, $q = 0$ belongs to this range. Then $1(= L^0) \sim C(L)L^{-\alpha(-\gamma_1+1)}$. Therefore, we can determine

$$C(L) \sim L^{\alpha-\alpha\gamma_1}. \tag{3}$$

Using Eq. (3), the dominant terms for all q ranges are

$$M_q \sim \begin{cases} L^{\alpha(1-\gamma_1)+D_f} V_{\min}^{q-\gamma_1+1} + L^{-\alpha q+D_f}, & (q < \gamma_1 - 1), \\ L^{-\alpha q+D_f}, & (\gamma_1 - 1 < q < \gamma_2 - 1), \\ L^{-\alpha(\gamma_2-1)+D_f-\beta(q-\gamma_2+1)}, & (\gamma_2 - 1 < q < \gamma_3 - 1), \\ L^{-\alpha(\gamma_2-1)+D_f-\beta(q-\gamma_2+1)}, & \\ +L^{-\alpha(\gamma_2-1)+D_f-\beta(\gamma_3-\gamma_2)} V_{\max}^{q-\gamma_3+1}, & (\gamma_3 - 1 < q), \end{cases} \tag{4}$$

where $V_{\min}$ and $V_{\max}$ are the minimum and maximum voltages in the voltage distribution with size L, respectively. Note that uttermost values $V_{\min}$ and $V_{\max}$ may originate from rare configurations which could be missed in Monte Carlo simulations. In addition, $V_{\min}$'s obtained in our simulation results for $L \geqslant 80$ cases are smaller than our simulation accuracy (10^{-10}), so it is hard to determine the correct size dependence of $V_{\min}$. Therefore, now we consider only the cases $\gamma_1 - 1 < q < \gamma_2 - 1$ and $\gamma_2 - 1 < q < \gamma_3 - 1$ and discuss the case $\gamma_3 - 1 < q$ later.

As seen in Eq. (4), the exponents are linear functions of q for the two q ranges. The slopes of the functions for $\gamma_1 - 1 < q < \gamma_2 - 1$ and $\gamma_2 - 1 < q < \gamma_3 - 1$ cases are $-\alpha$ and $-\beta$, which come from the two crossover voltages V_1 and V_2, respectively, and this constant gap scaling law fails at $q = \gamma_2 - 1$.

To confirm and demonstrate this analysis numerically, we consider the normalized moment $m_q \equiv (M_q/M_{q'})^{1/(q-q')}$, where q' is one of the values in the range to which q belongs. Using the estimated values $\gamma_1 \approx 0.19$, $\gamma_2 \approx 1.73$, and $\gamma_3 \approx 12$, we select $q' = 0$ and $q' = 5$ for $\gamma_1 - 1 < q < \gamma_2 - 1$ and $\gamma_2 - 1 < q < \gamma_3 - 1$ ranges, respectively. Then we obtain

$$m_q = \begin{cases} \left(\frac{M_q}{M_0}\right)^{1/q} \sim L^{-\alpha} & \text{for} \quad \gamma_1 - 1 < q < \gamma_2 - 1, \\ \left(\frac{M_q}{M_5}\right)^{1/(q-5)} \sim L^{-\beta} & \text{for} \quad \gamma_2 - 1 < q < \gamma_3 - 1. \end{cases} \tag{5}$$

According to Eq. (5), all the m_q belonging to the same (different) q range should scale identically (differently) with respect to the system size. Figure 4(a) shows the plot of m_q for several q values when $-0.81 < q < 0.73$ (blue symbols) as a function of L. All m_q are well fitted to the solid guide line with the slope $-\alpha = -1.82$. We also plot m_q for the case $0.73 < q < 11$ in Fig. 4(b). These data also agree well with the theoretical guide line with the slope $-\beta = -0.89$. We also plot the case $q > 11$ (green symbols) in Fig. 4(b), and it seems that m_q for $q > 11$ also follows the same guide line with slope -0.89, which indicates $V_{\max} \leqslant L^{-\beta}$. This shows that Region 3 retains its power law behavior only when $V_{\max} \sim L^{-\beta}$, whereas

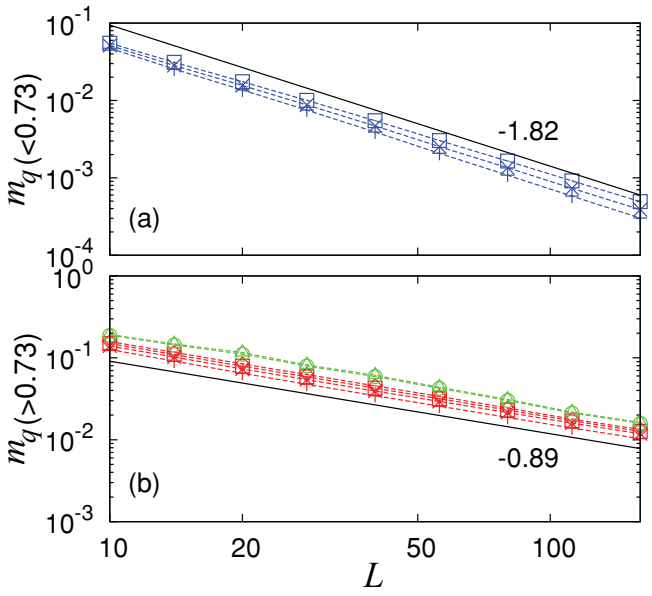

FIG. 4. (Color online) (a) Plot of m_q for several q values when $-0.82 < q < 0.73$ as a function of L. Data for $q = 0.1$, 0.3, and 0.5 are denoted by $+$, $\times$, and $\square$, respectively. The solid line is a guide line with a slope of -1.82. (b) Plot of m_q when $11 > q > 0.73$ (red symbols) against L for various q values: $q = 2.0$ ($+$), 4.0 ($\times$), 6.0 ($\square$), and 8.0 ($\diamond$). The slope of the solid guide line is -0.89. We also plot the case $q > 11$ (green symbols). $\circ$ and $\triangle$ symbols denote data for $q = 18$ and 20, respectively.

it collapses while approaching the thermodynamic limit or Region 3 is actually a (exponentially) decaying regime when $V_{\max} \ll L^{-\beta}$. However, in either case, the analytic results [Eqs. (4) and (5)] are valid for $q > \gamma_1 - 1$ because the contribution of a (exponentially) decaying function is negligible. These numerical results confirm that the moments of the voltage distribution is governed by the size-dependent behaviors of the characteristic voltages V_1 and V_2.

In summary, we have studied the voltage distribution of the two-dimensional dielectric breakdown network in which percolating cluster is formed dynamically. This distribution contains three distinctive power-law regions with different exponents γ_1, γ_2, and γ_3 which are divided by two crossover voltages V_1 and V_2. This multiple scaling behavior of the voltage distribution is different from that of the random resistor network, showing multifractal behaviors for which infinite exponents are needed. From the study of the size-dependent behavior of the voltage distribution, we obtained that the scaling relations of the qth moment as a function of L depend on q linearly and understand that the two crossover voltages determine different scaling behaviors of the qth moment, which are confirmed by numerical simulations. We think that the absence of the multifractal feature in the dielectric breakdown network is a result of a different mechanism generating the percolating structure. Since the conducting path is created by a driving antifuse dynamics, randomness is rather reduced. We expect that this work will help to understand not only the general statistical behaviors of the voltage distribution of the dielectric breakdown network but also how the dominant voltage scales with the system size. This is meaningful in the aspect that the random access memory (RAM) application based on the dielectric breakdown mechanism should be scaled to nano size for high-density memory [20,21], in which finite-size scaling properties become critical. From Eq. (4), resistance of the percolating cluster [7] $R \sim M_2^{-1} \sim L^{0.68}$. This means that ratio between percolating and broken cluster becomes larger as the system size decreases, which makes it much easier to distinguish 0 (broken) and 1 (percolating) states. In addition, noise power [7], $S_R \sim \sum_\alpha (i_\alpha/I)^4$ is proportional to $L^{0.26}$ for dielectric breakdown network, whereas $\sim L^{0.78}$ for the random resistor network, which indicates the noise power is less sensitive to the system size for the dielectric breakdown nework. This result indicates that the dielectric breakdown network-based RAM has advantages for the practical application.

This research was supported by the National Research Foundation of Korea (NRF) grant No. 2010-0015066 and by the NAP of the Korean Research Council of Fundamental Science & Technology (KRCF).

[1] D. Stauffer and A. Aharony, *Introduction to Percolation Theory*, revised 2nd ed. (Taylor & Francis, London, 1994).
[2] B. Kahng, Phys. Rev. Lett. **64**, 914 (1990).
[3] L. de Arcangelis, S. Redner, and A. Coniglio, Phys. Rev. B **31**, 4725 (1985).
[4] L. de Arcangelis, S. Redner, and A. Coniglio, Phys. Rev. B **34**, 4656 (1986).
[5] M. Barthélémy, S. V. Buldyrev, S. Havlin, and H. E. Stanley, Phys. Rev. E **61**, R3283 (2000).
[6] B. Fourcade, P. Breton, and A.-M. S. Tremblay, Phys. Rev. B **36**, 8925 (1987).
[7] R. Rammal, C. Tannous, and A.-M. S. Tremblay, Phys. Rev. A **31**, 2662 (1985).
[8] Y. Yagil, G. Deutscher, and D. J. Bergman, Phys. Rev. Lett. **69**, 1423 (1992).
[9] M. A. Dubson, Y. C. Hui, M. B. Weissman, and J. C. Garland, Phys. Rev. B **39**, 6807 (1989).
[10] H. E. Stanley and P. Meakin, Nature (London) **39**, 405 (1988).
[11] T. C. Halsey, M. H. Jensen, L. P. Kadanoff, I. Procaccia, and B. I. Shraiman, Phys. Rev. A **33**, 1141 (1986).
[12] H. Takayasu, Phys. Rev. Lett. **54**, 1099 (1985).
[13] S. C. Chae *et al.*, Adv. Mater. **20**, 1154 (2008).
[14] P. M. Duxbury, P. L. Leath, and P. D. Beale, Phys. Rev. B **36**, 367 (1987).
[15] B. Kahng, G. G. Batrouni, S. Redner, L. de Arcangelis, and H. J. Herrmann, Phys. Rev. B **37**, 7625 (1988).
[16] J. S. Lee *et al.*, Phys. Rev. Lett. **105**, 205701 (2010).
[17] R. Waser and M. Aono, Nat. Mater. **6**, 833 (2007).
[18] D.-H. Kwon *et al.*, Nat. Nanotech. **5**, 148 (2010).
[19] S. H. Chang *et al.*, Phys. Rev. Lett. **102**, 026801 (2009).
[20] M.-J. Lee *et al.*, Nano Lett. **9**, 1476 (2009).
[21] S.-E. Ahn *et al.*, Adv. Mater. **20**, 924 (2008).